Direct Observation of Degenerate Two-Photon Absorption and Its Saturation in WS_2 and MoS_2 Monolayer and Few-Layer Films

Saifeng Zhang,[†] Ningning Dong,[†] Niall McEvoy,[*,‡] Maria O'Brien,[‡,§] Sinéad Winters,[‡,§] Nina C. Berner,[‡] Chanyoung Yim,[‡,§] Yuanxin Li,[†] Xiaoyan Zhang,[†] Zhanghai Chen,[∥] Long Zhang,[†] Georg S. Duesberg,[‡,§] and Jun Wang[*,†,⊥]

[†]Key Laboratory of Materials for High-Power Laser, Shanghai Institute of Optics and Fine Mechanics, Chinese Academy of Sciences, Shanghai 201800, China, [‡]Centre for Research on Adaptive Nanostructures and Nanodevices (CRANN) and Advanced Materials and BioEngineering Research (AMBER) Centre, Trinity College Dublin, Dublin 2, Ireland, [§]School of Chemistry, Trinity College Dublin, Dublin 2, Ireland, [∥]State Key Laboratory of Surface Physics, Key Laboratory of Micro and Nano Photonic Structures (Ministry of Education), Department of Physics, Fudan University, Shanghai 200433, People's Republic of China, and [⊥]State Key Laboratory of High Field Laser Physics, Shanghai Institute of Optics and Fine Mechanics, Chinese Academy of Sciences, Shanghai 201800, China

ABSTRACT The optical nonlinearity of WS_2 and MoS_2 monolayer and few-layer films was investigated using the *Z*-scan technique with femtosecond pulses from the visible to the near-infrared range. The nonlinear absorption of few- and multilayer WS_2 and MoS_2 films and their dependences on excitation wavelength were studied. WS_2 films with 1−3 layers exhibited a giant two-photon absorption (TPA) coefficient as high as $(1.0 \pm 0.8) \times 10^4$ cm/GW. TPA saturation was observed for the WS_2 film with 1−3 layers and for the MoS_2 film with 25−27 layers. The giant nonlinearity of WS_2 and MoS_2 films is attributed to a two-dimensional confinement, a giant exciton effect, and the band edge resonance of TPA.

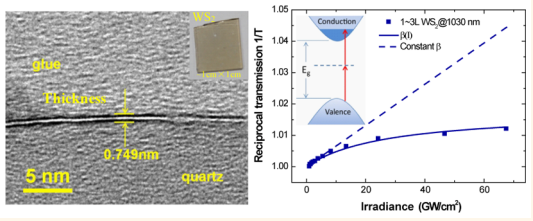

KEYWORDS: two-photon absorption · saturable absorption · WS_2 · MoS_2 · two-dimensional semiconductors · *Z*-scan

Investigation of nonparametric processes concerning nonlinear absorption in transition metal dichalcogenides (TMDs) has revealed a new category of photonic nanomaterials with potential applications in optical switching, mode-locking, and optical limiting.[1−9] Unlike gapless graphene, monolayer TMDs possess a direct band gap. Combined with the advantage of monomolecular layer thickness, the X−M−X sandwich structure, where M stands for a transition metal (*e.g.*, Mo, W, Ti, or Nb) and X stands for a chalcogen (*e.g.*, S, Se, or Te), behaves like a natural semiconductor quantum well. Electrons are closely confined in a two-dimensional (2D) plane, implying significant enhancement of optical nonlinearity in these ultrathin semiconductors.[10−16]

In this paper, we show that monolayer and few-layer WS_2 and MoS_2 films exhibit strong two-photon absorption (TPA) for femtosecond pulses at 1030 nm. The dependence of the optical absorption nonlinearity on the number of layers (WS_2: 1−3 layers (L), 18−20L, 39−41L; MoS_2: 25−27L, 72−74L) and the excitation wavelength (1030, 800, and 515 nm) was investigated. Saturation of TPA was observed for the WS_2 film with 1−3L and for the MoS_2 film with 25−27L at 1030 nm. According to a hyperbolic TPA saturation model, the estimated TPA coefficient for the 1−3L WS_2 film at 1030 nm was deduced to be $(1.0 \pm 0.8) \times 10^4$ cm/GW, much larger than that of common bulk semiconductors such as GaAs, CdS, and ZnO. This giant TPA coefficient was attributed to a 2D confinement of electrons, a giant exciton effect, and the band edge resonance of TPA.

RESULTS AND DISCUSSION

The WS_2 and MoS_2 films were synthesized by direct vapor phase sulfurization of predeposited metal films in a quartz tube furnace with two temperature zones as reported previously.[17,18] Thin metal films

* Address correspondence to jwang@siom.ac.cn, nmcevoy@tcd.ie.

Received for review March 26, 2015 and accepted July 2, 2015.

Published online July 02, 2015
10.1021/acsnano.5b03480

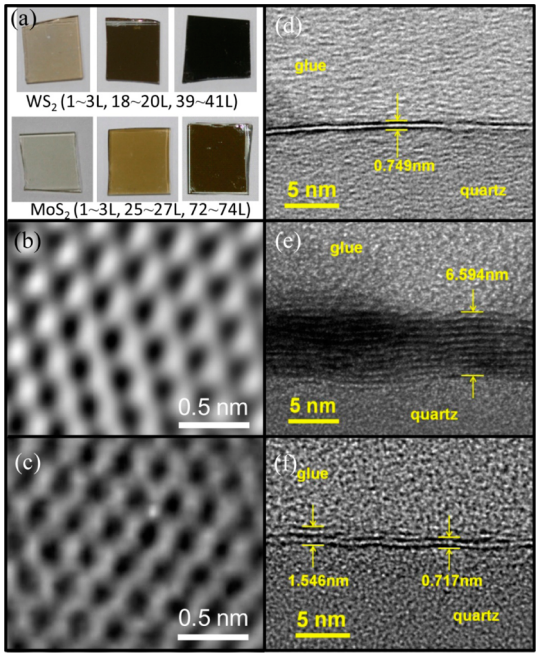

Figure 1. (a) Photographs of 1−3L, 18−20L, and 39−41L WS_2 films and 1−3L, 25−27L, and 72−74L MoS_2 films. In-plane TEM of (b) 1−3L WS_2 film and (c) 1−3L MoS_2 film. Cross-sectional TEM of the (d) 1−3L and (e) 8−10L WS_2 films and (f) 1−3L MoS_2 film.

(W, Mo, 99.99% MaTecK) were sputtered onto fused quartz substrates (~10 mm × 10 mm, Alfa Aesar) using a Gatan precision etching coating system with a quartz crystal microbalance to monitor the W or Mo thickness. Four types of samples with initial metal film thicknesses of 0.5, 1, 5, and 20 nm were prepared. They were heated to 750 °C in the hot zone and annealed for 30 min under Ar flow. Then sulfur powder (MaTecK, 99%) in the upstream temperature zone was heated to its melting point (~113 °C), and the sulfur vapor was transported to the predeposited metal films by the carrier gas (Ar). After sulfurization, the samples were held at 750 °C for 20 min and then cooled to room temperature. Photographs of the WS_2 and MoS_2 films (initial W or Mo layer thicknesses: 0.5, 5, and 20 nm) on quartz substrates are shown in Figure 1a. The samples with different thicknesses of predeposited metal films are clearly distinguishable from each other. All samples appear uniform over the entire area of ~10 mm × 10 mm. Figure 1b,c shows the in-plane high-resolution transmission electron microscopy (HRTEM) images of WS_2 and MoS_2 films. In both images, the hexagonal lattice structures reveal a good crystalline quality of the samples. To determine the number of layers, we utilized cross-sectional TEM for the thin samples (initial W or Mo layer thickness: 0.5 and 1 nm) and spectroscopic ellipsometry (SE) for the relatively thick samples (initial W or Mo layer thickness: 5 and 20 nm). The cross-sectional TEM images of WS_2 (initial W: 0.5 and 1 nm) and MoS_2 (initial Mo layer thickness: 0.5 nm) films were obtained by plasma etching and are shown in Figure 1d−f. It is clear that the monolayer thickness is ~0.75 nm for WS_2 and ~0.72 nm for MoS_2, which agrees well with the reported atomic force microscopy results.[19−22] The cross-sectional TEM images suggest that the 1−3L WS_2 film consists mostly of a monolayer, while a monolayer and a bilayer coexist in the 1−3L MoS_2 film. The number of layers in the thicker samples (initial W or Mo layer thickness: 5 and 20 nm) after sulfurization was confirmed by SE, similar to our previously reported results.[23] The initial nominal thicknesses of the predeposited metal films, the thicknesses after sulfurization, and the number of layers are listed in Table 1.

TABLE 1. Number of Layers in the WS_2 and MoS_2 Films

M = W, Mo X = S	initial nominal M (nm)	measured MX_2 (nm)	MX_2 layer number (L)
W	0.5	0.75−2.25	1−3
	5	13.5−15.0	18−20
	20	29.25−30.75	39−41
Mo	0.5	0.72−2.16	1−3
	5	18−19.44	25−27
	20	51.84−53.28	72−74

Raman spectroscopy was employed to examine the crystallinity and number of layers. The measurements were carried out using a Renishaw inVia Raman spectrometer with a laser at 488 nm. As shown in Figure 2a, b, there are two optical phonon modes E^1_{2g} and A_{1g} for all WS_2 and MoS_2 films, where E^1_{2g} corresponds to an in-plane optical mode and A_{1g} is an out-of-plane vibration along the *c*-axis direction of the layers. Notably, the Raman peaks shift with increasing number of layers. The frequency difference between E^1_{2g} and A_{1g} varies from 63.4 to 65.3 cm^{-1} when the number of layers of WS_2 films increases from 1−3L to 39−41L, while it varies from 19.4 to 26.6 cm^{-1} for MoS_2 films from 1−3L to 72−74L. The positions of all Raman peaks are in good agreement with reported results.[19,24−26] The strong PL signal shown in our previous work also indicates a good uniformity of the film.[18]

X-ray photoelectron spectroscopy (XPS) spectra were recorded on a VG Scientific ESCAlab MkII system using Al Kα X-rays and an analyzer pass energy of 20 eV. In Figure 2c, the deconvolution of the W 4f and W $5p_{3/2}$ core-level regions reveals the surface tungsten as predominantly in WS_2, with only a small component at a lower binding energy, which indicates traces of unsulfurized or substoichiometric W. The Mo 3d core level in Figure 2d was successfully fitted with only one Mo component corresponding to MoS_2. Neither the W 4f nor the Mo 3d core levels show signs of significant amounts of oxides, further indicating the high quality of the films.

To obtain the linear absorption coefficients of the WS_2 and MoS_2 films, we measured the reflection (*R*) and transmission (*T*) spectra for wavelengths in the 500−1100 nm range using a PerkinElmer Lambda

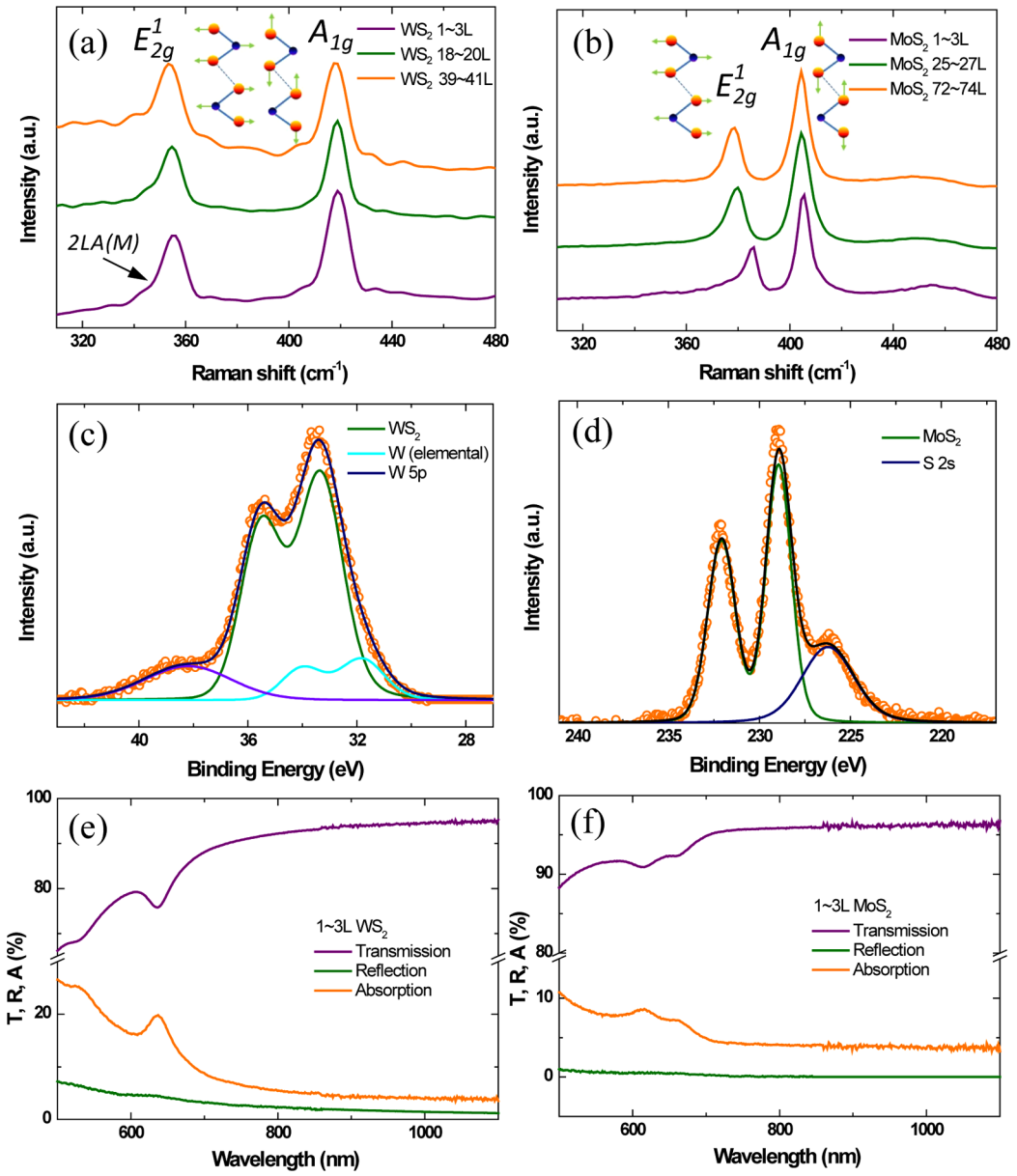

Figure 2. Raman spectra of (a) WS_2 and (b) MoS_2 films and XPS of (c) WS_2 and (d) MoS_2 films. Transmission, reflection, and absorption spectra of (e) 1−3L WS_2 film and (f) 1−3L MoS_2 film.

1050 UV/vis/NIR spectrophotometer equipped with an integrating sphere accessory. The absorption spectra *A* were obtained *via* the formula $A = 1 - R - T$. In Figure 2e, the transmission of the 1−3L WS_2 film in the near-infrared range is above 90%, and it decreases steeply in the visible range, while the reflection increases gradually from 1.2% at 1100 nm to 7.0% at 500 nm. The absorption in the near-infrared range far from the exciton resonance peak is about 4%, nearly two times larger than that of graphene (∼2.3%). The A (636.4 nm, 1.95 eV) and B (528.2 nm, 2.35 eV) exciton peaks for the 1−3L WS_2 film can be seen from the transmission and absorption curves. In Figure 2f, compared to WS_2, the transmission and reflection spectra of the 1−3L MoS_2 film exhibit relatively smooth features, above 90% for *T* throughout the entire range and from about 0.04% at 1100 nm to 0.8% at 500 nm for *R*. The absorption in the near-infrared range is about 3.8%, slightly smaller than that for the WS_2 film. The exciton peaks of A (662.5 nm, 1.87 eV) and B (615.0 nm, 2.02 eV) for the 1−3L MoS_2 film can also be found in the transmission and absorption curves.

The nonlinear optical (NLO) properties of the WS_2 and MoS_2 films were investigated using an open aperture *Z*-scan system with femtosecond laser pulses at 1030, 800, and 515 nm. The pulse width of a fiber laser source at 1030 nm (double frequency at 515 nm) was ∼340 fs with a repetition rate of 100 Hz, while the excitation laser at 800 nm was a Ti:sapphire-type (pulse width = 40 fs, repetition rate = 1000 Hz, Coherent Co.). The reference beam of incident light and the transmitted beam were monitored by two photodiodes as

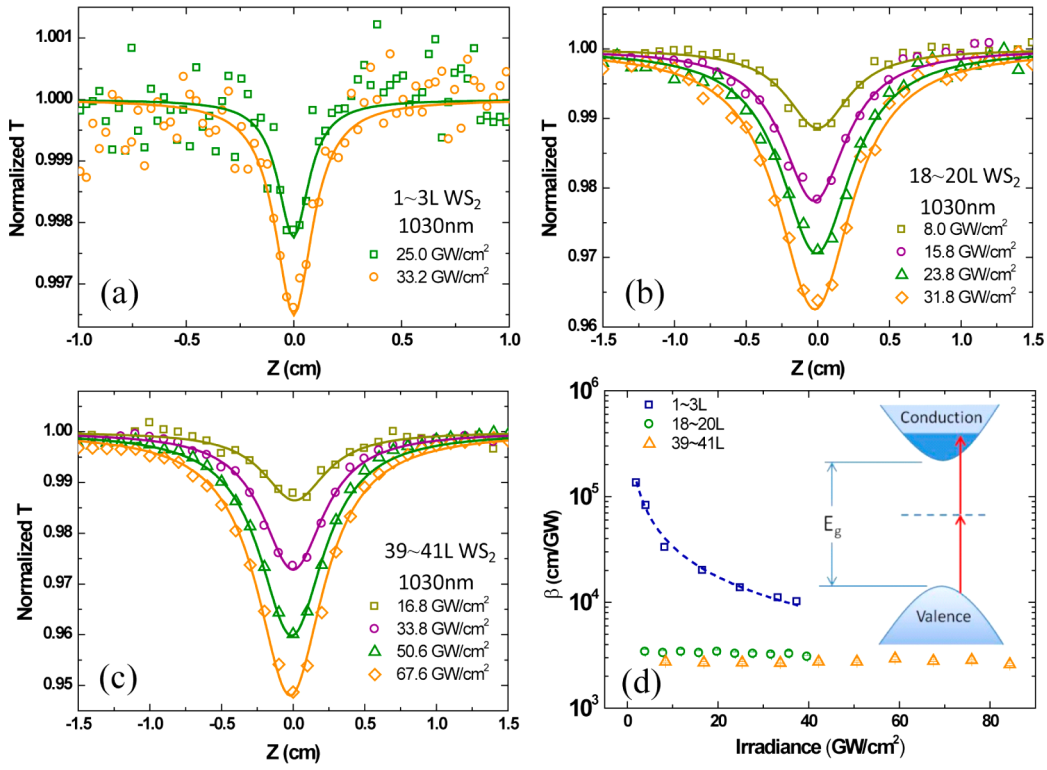

Figure 3. *Z*-scan results for the WS_2 films with (a) 1−3L, (b) 18−20L, (c) 39−41L, and (d) corresponding TPA coefficients. Inset: Schematic of TPA saturation (excitation laser = 1030 nm, 340 fs).

the sample moved through the focus of a lens along the laser propagation direction. The precision of the experimental setup was confirmed by our previous measurements of graphene/PVA films and MoS_2 nanoflake suspensions.[2,3,27] For example, the figure of merit (FOM) = $|\mathrm{Im}\chi^{(3)}/\alpha_0|$ of graphene/PVA films was about $(9.3 \pm 4.4) \times 10^{-15}$ esu cm, in a good agreement with the reported result of $\sim 5.0 \times 10^{-15}$ esu cm.[28] Figure 3a−c shows the *Z*-scan data of the 1−3L, 18−20L, and 39−41L of WS_2 films excited by 1030 nm (340 fs) laser pulses at different intensities. The NLO response of the 1−3L WS_2 film emerges at 2.08 GW/cm^2 and the amplitude becomes maximal (~0.35%) at ~38 GW/cm^2. The damage threshold at 1030 nm is about 68 GW/cm^2. At irradiance above this threshold, the 1−3L WS_2 film is destroyed and the *Z*-scan curve increases abruptly. Figure 3a shows the typical *Z*-scan curves of the 1−3L WS_2 film at 1030 nm. It is reasonable to assume that TPA occurs in the 1−3L WS_2 film as its band gap is about 1.9 eV,[22] larger than the energy of one photon (1.204 eV) but smaller than the energy of two photons (2.408 eV) of the laser beam at 1030 nm. In what follows, this reasoning is confirmed by the results of theoretical fitting using the nonlinear absorption model. As shown in Figure 3b,c, the 18−20L and 39−41L WS_2 films also exhibit the TPA response at 1030 nm as the band gap decreases to about 1.3 eV when the number of layers in the WS_2 films increases toward bulk.[29−31] The corresponding damage thresholds are about 40 and 84 GW/cm^2 for the 18−20L and 39−41L WS_2 films, respectively. The minimum of normalized transmission increases from ~0.35 to ~5.3% when the number of layers increases from 1−3L to 39−41L, indicating the dependence of NLO response on the number of layers.

To quantitatively determine the TPA property of the WS_2 films, the *Z*-scan data were fitted by assuming the nonlinear absorption model.[32]

$$\frac{dI(z')}{dz'} = -\alpha_0 I(z') - \beta I^2(z') \quad (1)$$

where $I(z')$ is the laser beam irradiance within the sample, z' is the propagation distance in the sample, α_0 is the linear absorption coefficient of the sample, and β is the second-order absorption coefficient. For TPA, β is positive, while for saturable absorption (SA), β is negative. This equation can be solved exactly, and the normalized power transmission is

$$T(z) = \frac{\ln[1 + q_0(z)]}{q_0(z)} \quad (2)$$

where $q_0(z) = \beta(I_0 L_{\mathrm{eff}})/(1 + z^2/z_0^2)$, $L_{\mathrm{eff}} = (1 - e^{-\alpha_0 L})/\alpha_0$ is the sample's effective thickness, I_0 is the on-axis irradiance at the focus, z_0 is the beam's diffraction length, and R is the reflection of the sample. It is worth noting that the reflection is taken into account in the model because, according to the results in Figure 2e,f, it cannot be neglected. In eq 1, we have excluded the second harmonic generation (SHG) effect in the WS_2 and MoS_2 films (odd number of layers).[33−38] According

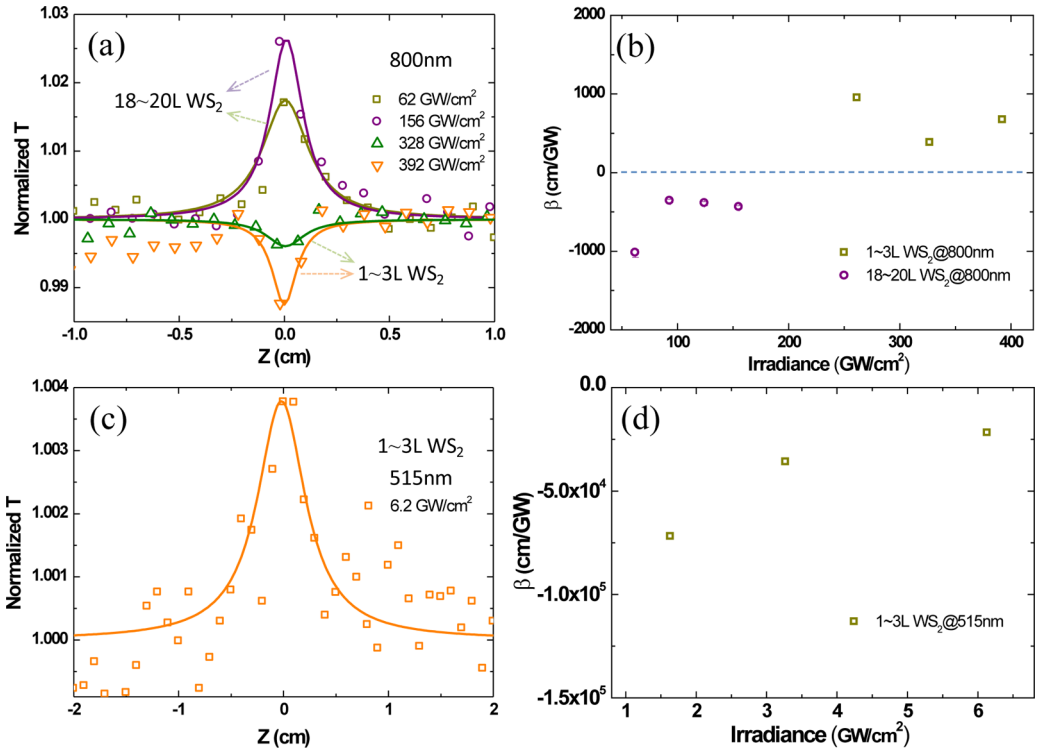

Figure 4. *Z*-scan results (a) and nonlinear absorption coefficients (b) for WS_2 films with 1−3L and 18−20L at 800 nm (40 fs). *Z*-scan results (c) and SA coefficients (d) for 1−3L WS_2 at 515 nm (340 fs).

to the results of Janisch *et al.*,[33] the SHG conversion efficiency of a suspended WS_2 monolayer is about 10^{-5}, which is 2−3 orders of magnitude smaller than the variation of the normalized transmission (about 10^{-3} to 10^{-2}) in our *Z*-scan experiments. In order to figure out the pure SHG signal from the transmitted beam, we placed an 850 nm short-pass filter for blocking the fundamental frequency beam (1030 nm). We found that all the *Z*-scan curves for 1−3L, 18−20L, and 39−41L WS_2 films were almost flat, indicating that the SHG effect was negligible compared with the TPA effect (see Supporting Information Figure S2). In addition, the TPA-generated free carrier absorption (FCA) effect can be neglected. The critical fluence F_c ($F_c = 4\sqrt{2}\hbar\omega[\sigma(1 - R)]$, where σ is the FCA absorption cross section) for FCA effect is much lower when compared to the onset fluence for TPA.[39] According to ref 2, the estimated F_c is ~0.1 J/cm^2, approximately 1 order of magnitude larger than the fluence in our experiment.

The solid curves in Figure 3a−c are the fitting results based on the nonlinear absorption model and agree well with the experimental data. The TPA coefficients for the 1−3L, 18−20L, 39−41L WS_2 films at 1030 nm were extracted and are shown in Figure 3d. For the 1−3L WS_2 film, the TPA coefficient is ~1.34×10^5 cm/GW at ~2.08 GW/cm^2, and it decreases monotonically to ~1.06×10^4 cm/GW at ~38 GW/cm^2. This reduction is ascribed to the saturation of TPA, and it will be discussed in detail in what follows. For the 18−20L and 39−41L WS_2 films, they turn out to be indirect semiconductors and at all intensities the TPA coefficients remain nearly constant, ~3280 and 2750 cm/GW, respectively. Notably, the TPA coefficient of the 1−3L WS_2 film is about 1 order of magnitude larger than those of the 18−20L and 39−41L WS_2 films, which is probably due to the transition from direct to indirect band gap caused by an interlayer interaction. Compared with many other bulk semiconductors such as ZnTe, CdTe, GaAs, and ZnO, the TPA coefficients of monolayer and few-layer WS_2 films at 1030 nm are about ~10^3 to 10^4 times larger[40,41] and are comparable to monolayer and bilayer graphene at ~1 μm.[42] It is worth noting that the TPA coefficient of WS_2 films does not obey the scaling rule applicable to many semiconductors, as proposed by Van Stryland.[40] This is attributed to the 2D confinement of layered WS_2, a giant exciton effect,[43,44] and the resonance of TPA near the band edge.

To investigate the wavelength dependence of NLO response of the WS_2 films, we obtained the *Z*-scan results at 800 nm (40 fs) and 515 nm (340 fs). As shown in Figure 4a, the NLO responses of the 1−3L and 18−20L WS_2 films at 800 nm (1.55 eV) are obviously different. The 1−3L WS_2 film retains TPA behavior the same as that at 1030 nm, but the 18−20L film exhibits the SA response. The TPA excitation irradiance for the 1−3L WS_2 film at 800 nm is larger than that at 1030 nm by about 1 order of magnitude. It may be due to the larger shift from TPA resonance of the band edge at 800 nm. The SA behavior of the 18−20L sample implies

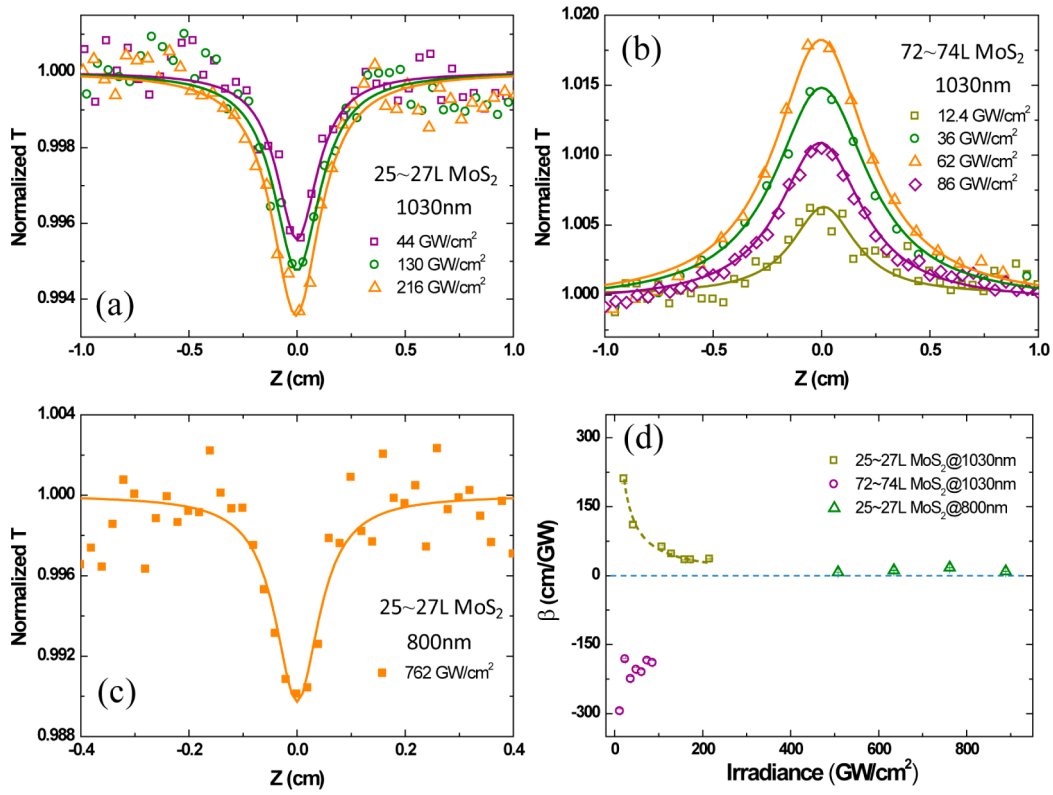

Figure 5. *Z*-scan results for the MoS_2 films with (a) 25−27L, (b) 72−74L (excitation laser = 1030 nm, 340 fs), and (c) 25−27L (excitation laser = 800 nm, 40 fs). (d) Corresponding nonlinear absorption coefficients.

that its band gap is smaller than 1.55 eV, and the SA induced by one-photon absorption takes place. The damage thresholds of the 1−3L and 18−20L WS_2 films at 800 nm are close to 392 and 156 GW/cm^2, respectively. The experimental data are fitted by the nonlinear absorption model mentioned above. The obtained TPA and SA coefficients are shown in Figure 4b, showing a weak saturation effect similar to that for the 1−3L WS_2 film at 1030 nm. In Figure 4c, the 1−3L WS_2 film at 515 nm (2.408 eV) starts to exhibit the SA behavior at a much lower irradiance, which is caused by one-photon absorption, as well.

Figure 5 shows the dependence of NLO response on the number of layers and excitation wavelength for the 25−27L and 72−74L MoS_2 films at 1030 and 800 nm. Similar to the WS_2 films, the band gap of the MoS_2 films also decreases with increasing number of layers, from 1.90 eV for the monolayer to 1.29 eV for the bulk.[45,46] In Figure 5a,b, at 1030 nm, the 25−27L MoS_2 film exhibits TPA behavior, whereas the behavior of the 72−74L one changes to SA at a lower irradiance induced by one-photon absorption. This implies that the band gap of the 25−27L MoS_2 film is larger than 1.55 eV, while that of the 72−74L one is smaller. The damage thresholds of the 25−27L and 72−74L MoS_2 films at 1030 nm are close to ∼360 and ∼86 GW/cm^2, respectively. In Figure 5c, at 800 nm, the 25−27L MoS_2 film still exhibits the TPA behavior, but the excitation irradiance is much larger than that at 1030 nm in Figure 5a. This phenomenon also reveals that the ON/OFF resonance of TPA near the band edge plays an important role in the NLO response. The damage threshold of the 25−27L MoS_2 film at 800 nm is close to ∼888 GW/cm^2. The TPA coefficients of the 25−27L MoS_2 film at 1030 and 800 nm are shown in Figure 5d. At 1030 nm, it decreases monotonically from 210 to 34.7 cm/GW due to the TPA saturation. The TPA coefficient at 1030 nm is larger than that at 800 nm for the 25−27L MoS_2 film and remains nearly constant at ∼11.4 cm/GW at 800 nm, confirming the importance of resonance for NLO response. The SA coefficient of the 72−74L MoS_2 film at 1030 nm is about −250 ± 50 cm/GW, as shown in Figure 5d.

In eq 1, the nonlinear absorption coefficient β is assumed to be independent of the irradiance, and this is valid only at low intensities. When the TPA saturation occurs, the nonlinear absorption coefficient is supposed to be dependent on the irradiance. The TPA saturation of the WS_2 and MoS_2 films can be well fitted by using a hyperbolic saturation model for semiconductors:[47,48]

$$\beta(I) = \frac{\beta_0}{1 + I/I_{sat}} \tag{3}$$

where β_0 is the low irradiance response of the material and I_{sat} is the saturation irradiance of TPA for which β_0 is divided by 2. With eq 3, we can solve eq 1 numerically and obtain the relationship between the reciprocal

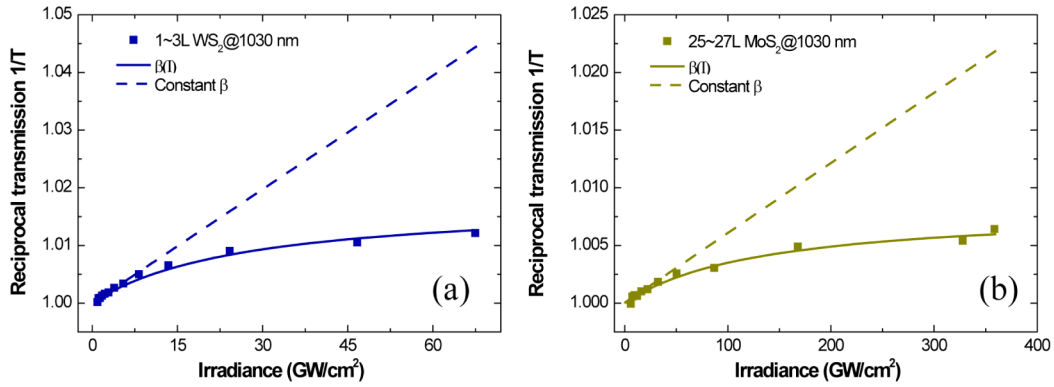

Figure 6. Reciprocal transmission *versus* irradiance of (a) 1−3L WS_2 film and (b) 25−27L MoS_2 film. Solid squares are the measured data. Solid line: theoretical variation for a hyperbolic irradiance dependence of the TPA coefficient. Dashed line: theoretical variation for a constant TPA coefficient.

TABLE 2. Linear and NLO Parameters of Few-Layer WS_2 and MoS_2 Films Measured Using the *Z*-Scan Technique

laser	sample	T (%)	α_0 (cm^{-1})	NLO response	β (cm GW^{-1})	I_{sat} of TPA (GW cm^{-2})	Im$\chi^{(3)}$ (esu)	FOM (esu cm)	damage threshold I_d (GW cm^{-2})
1030 nm, 1 kHz, 340 fs	1−3L WS_2	94.76	7.17×10^5	TPA	$(1.0 \pm 0.8) \times 10^4$	26	$(4.0 \pm 3.6) \times 10^{-8}$	$(1.1 \pm 1.0) \times 10^{-13}$	~68
	18−20L WS_2	42.64	5.98×10^5	TPA	$(3.28 \pm 0.11) \times 10^3$	N/A	$(1.29 \pm 0.04) \times 10^{-8}$	$(2.16 \pm 0.08) \times 10^{-14}$	~40
	39−41L WS_2	7.65	8.57×10^5	TPA	$(2.75 \pm 0.10) \times 10^3$	N/A	$(1.10 \pm 0.04) \times 10^{-8}$	$(1.28 \pm 0.05) \times 10^{-14}$	~84
	25−27L MoS_2	92.96	3.90×10^4	TPA	66 ± 4	130	$(4.2 \pm 0.2) \times 10^{-10}$	$(1.10 \pm 0.03) \times 10^{-14}$	~360
	72−74L MoS_2	37.01	1.89×10^5	SA	-250 ± 50	N/A	$(-1.50 \pm 0.33) \times 10^{-9}$	$(7.96 \pm 1.68) \times 10^{-15}$	~86
800 nm, 1 kHz, 40 fs	1−3L WS_2	92.21	1.08×10^6	TPA	525 ± 205	N/A	$(2.72 \pm 0.83) \times 10^{-9}$	$(2.51 \pm 0.77) \times 10^{-15}$	~392
	18−20L WS_2	35.75	7.22×10^5	SA	-397 ± 40	N/A	$(-1.78 \pm 0.16) \times 10^{-9}$	$(2.47 \pm 0.23) \times 10^{-15}$	~156
	25−27L MoS_2	88.98	6.24×10^4	TPA	11.4 ± 4.3	N/A	$(5.26 \pm 2.46) \times 10^{-11}$	$(8.43 \pm 3.95) \times 10^{-16}$	~888
515 nm, 1 kHz, 340 fs	1−3L WS_2	67.80	5.18×10^6	SA	$(-2.9 \pm 1.0) \times 10^4$	N/A	$(-8.44 \pm 3.80) \times 10^{-8}$	$(1.63 \pm 0.73) \times 10^{-14}$	~6.2

transmission $1/T$ and irradiance. Figure 6a,b shows reciprocal transmission *versus* irradiance of the 1−3L WS_2 film and 25−27L MoS_2 film, respectively. The solid squares denote the measured data. The solid line is the theoretical variation for a hyperbolic irradiance dependence of the TPA coefficient, whereas the dashed line is the theoretical variation for a constant TPA coefficient. From the fits, we obtain $\beta_0 = \beta(I \ll I_{sat}) = (1.0 \pm 0.8) \times 10^4$ cm GW^{-1}, $I_{sat} = 26$ GW cm^{-2} for the 1−3L WS_2 film and $\beta_0 = 66 \pm 4$ cm GW^{-1}, $I_{sat} = 130$ GW cm^{-2} for the 25−27L MoS_2 film at 1030 nm. The TPA coefficient of the 25−27L MoS_2 film is much smaller than that of the monolayer MoS_2, $(7.62 \pm 0.15) \times 10^3$ cm GW^{-1}.[49] Recently, MoS_2 and WS_2 films have been demonstrated successfully as saturable absorbers for mode-locking or Q-switching in ultrafast fiber lasers over a broad wavelength range (1, 1.5, and 2 μm). However, the mechanism of such a saturable absorber working below the band gap is still unclear. Wang[5] and Woodward *et al.*[50] ascribed it to defect state or edge state saturable absorption. On the basis of our results, it is reasonable to deduce that the TPA saturation should be easier to achieve for fewer-layer films, and it might be one factor for the monolayer and few-layer WS_2 and MoS_2 working as saturable absorbers below the band gap.

Table 2 summarizes the linear and NLO parameters of the WS_2 and MoS_2 films measured by using the *Z*-scan technique. The imaginary part of the third-order NLO susceptibility Im$\chi^{(3)}$ can be approximately expressed:[2]

$$\mathrm{Im}\,\chi^{(3)} = \frac{10^{-7} c\lambda n^2}{96\pi^2}\beta \qquad (4)$$

where c is the speed of light, λ is the wavelength of the incident light, and n is the refractive index. The linear refractive indices of the WS_2 and MoS_2 films at 1030 nm were obtained from a Cauchy dispersion formula based on the results of Li *et al.*[51] The figure of merit was defined for eliminating the discrepancy caused by the linear absorption α_0: FOM = |Im$\chi^{(3)}/\alpha_0$|. Im$\chi^{(3)}$ of the 1−3L WS_2 film at 1030 nm is $(4.0 \pm 3.6) \times 10^{-8}$ esu, about 3-fold larger than the values for 18−20L and 39−41L ones. Im$\chi^{(3)}$ of the 1−3L WS_2 film at 800 nm is 1 order of magnitude smaller than that at 1030 nm, indicating the OFF resonance of TPA near the band edge. Im$\chi^{(3)}$ changes from positive to negative for the 18−20L WS_2 film due to the transition from TPA to SA.

The FOM exhibits similar behavior. For the 25−27L MoS_2 film at 1030 nm, $\mathrm{Im}\chi^{(3)}$ is $(4.2 \pm 0.2) \times 10^{-10}$ esu, about 1 order of magnitude larger than that at 800 nm, which is also ascribed to the band edge TPA resonance. For the 72−74L MoS_2 film, it becomes negative at 1030 nm due to SA.

CONCLUSIONS

In conclusion, we investigated the optical nonlinearity of monolayer and few-layer WS_2 and MoS_2 films by using the *Z*-scan technique at 1030, 800, and 515 nm with femtosecond pulses. The 2D 1−3L WS_2 film exhibits giant optical nonlinearities with a TPA coefficient of $(1.0 \pm 0.8) \times 10^4$ cm/GW. The nonlinear absorption of few- and multilayer WS_2 and MoS_2 films and their excitation wavelength dependences were studied. The saturation of TPA was observed for the 1−3L WS_2 film and 25−27L MoS_2 film. The giant nonlinearity of WS_2 and MoS_2 films was ascribed to the 2D confinement, giant exciton effect, and the band edge resonance of TPA. The damage thresholds of the WS_2 and MoS_2 films were also estimated to support potential device application in the future.

METHODS

Spectroscopic Ellipsometry. Spectroscopic ellipsometry was employed to measure the thicknesses of MoS_2 and WS_2 films.[23,52] An Alpha SE tool (J.A. Woollam Co., Inc.) was used, and SE data were obtained in the wavelength range of 380−900 nm at 65 and 70° angles of incidence, with a beam spot size of ~40 mm^2. The SE spectra were analyzed by using vender-supplied software, CompleteEASE 4.72 (J.A. Woollam Co., Inc.).

The measured SE spectra consist of psi (Ψ) and delta (Δ) components, which represent the amplitude ratio (Ψ) and phase difference (Δ) between p- and s-polarizations, respectively. The two parameters are related to the ratio ρ, defined by the equation of $\rho = r_p/r_s = \tan(\Psi)\exp(i\Delta)$, where r_p and r_s are the amplitude reflection coefficients for the p-polarized and s-polarized light, respectively.[53]

Optical models built for SE analysis have a four-layered structure, where there are three sublayers (a Si substrate, an interface layer between the Si and SiO_2 layers, and a SiO_2 layer) and a top material layer (MoS_2 or WS_2). The Tauc-Lorentz oscillation model was used to determine the thicknesses of the MoS_2/WS_2 thin films.[54]

Conflict of Interest: The authors declare no competing financial interest.

Acknowledgment. The authors thank NSFC funds (Nos. 61308034 and 61178007), STCSM (No. 12ZR1451800), and the External Cooperation Program of BIC, CAS (No. 181231KYSB20130007) for support. N.M.E. acknowledges SFI for 14/TIDA/2329. M.O., S.W., N.C.B., C.Y., and G.S.D. acknowledge SFI for PI_10/IN.1/I3030. L.Z. thanks the Excellent Academic Leader of Shanghai (No. 10XD1404600) for support. J.W. thanks the National 10000-Talent Program for financial support and acknowledges Prof. Werner J. Blau at Trinity College Dublin for his helpful discussion in this work.

Supporting Information Available: Additional figures to exclude the SHG effect in the experiment. The Supporting Information is available free of charge on the ACS Publications website at DOI: 10.1021/acsnano.5b03480.

REFERENCES AND NOTES

1. Tsai, D.-S.; Liu, K.-K.; Lien, D.-H.; Tsai, M.-L.; Kang, C.-F.; Lin, C. A.; Li, L.-J.; He, J.-H. Few-Layer MoS_2 with High Broadband Photogain and Fast Optical Switching for Use in Harsh Environments. *ACS Nano* **2013**, *7*, 3905–3911.
2. Wang, K.; Wang, J.; Fan, J.; Lotya, M.; O'Neil, A.; Fox, D.; Feng, Y.; Zhang, X.; Jiang, B.; Zhao, Q.; et al. Ultrafast Saturable Absorption of Two-Dimensional MoS_2 Nanosheets. *ACS Nano* **2013**, *7*, 9260–9267.
3. Wang, K.; Feng, Y.; Chang, C.; Zhan, J.; Wang, C.; Zhao, Q.; Coleman, J. N.; Zhang, L.; Blau, W. J.; Wang, J. Broadband Ultrafast Nonlinear Absorption and Nonlinear Refraction of Layered Molybdenum Dichalcogenide Semiconductors. *Nanoscale* **2014**, *6*, 10530–10535.
4. Kassani, S. H.; Khazaeinezhad, R.; Jeong, H.; Nazari, T.; Yeom, D.-I.; Oh, K. All-Fiber Er-Doped Q-Switched Laser Based on Tungsten Disulfide Saturable Absorber. *Opt. Mater. Express* **2015**, *5*, 373–379.
5. Wang, S.; Yu, H.; Zhang, H.; Wang, A.; Zhao, M.; Chen, Y.; Mei, L.; Wang, J. Broadband Few-Layer MoS_2 Saturable Absorbers. *Adv. Mater.* **2014**, *26*, 3538–3544.
6. Zhang, H.; Lu, S. B.; Zheng, J.; Du, J.; Wen, S. C.; Tang, D. Y.; Loh, K. P. Molybdenum Disulfide (MoS_2) As a Broadband Saturable Absorber for Ultra-Fast Photonics. *Opt. Express* **2014**, *22*, 7249–7260.
7. Fu, X.; Qian, J.; Qiao, X.; Tan, P.; Peng, Z. Nonlinear Saturable Absorption of Vertically Stood WS_2 Nanoplates. *Opt. Lett.* **2014**, *39*, 6450–6453.
8. Mao, D.; Wang, Y.; Ma, C.; Han, L.; Jiang, B.; Gan, X.; Hua, S.; Zhang, W.; Mei, T.; Zhao, J. WS_2 Mode-Locked Ultrafast Fiber Laser. *Sci. Rep.* **2015**, *5*, 7965.
9. Loh, K. P.; Zhang, H.; Chen, W. Z.; Ji, W. Templated Deposition of MoS_2 Nanotubules Using Single Source Precursor and Studies of Their Optical Limiting properties. *J. Phys. Chem. B* **2006**, *110*, 1235–1239.
10. Yin, X.; Ye, Z.; Chenet, D. A.; Ye, Y.; O'Brien, K.; Hone, J. C.; Zhang, X. Edge Nonlinear Optics on a MoS_2 Atomic Monolayer. *Science* **2014**, *344*, 488–490.
11. Kumar, N.; Najmaei, S.; Cui, Q.; Ceballos, F.; Ajayan, P. M.; Lou, J.; Zhao, H. Second Harmonic Microscopy of Monolayer MoS_2. *Phys. Rev. B: Condens. Matter Mater. Phys.* **2013**, *87*, 161403(R).
12. Janisch, C.; Wang, Y.; Ma, D.; Mehta, N.; Elías, A. L.; Perea-López, N.; Terrones, M.; Crespi, V.; Liu, Z. Extraordinary Second Harmonic Generation in Tungsten Disulfide Monolayers. *Sci. Rep.* **2014**, *4*, 5530.
13. Malard, L. M.; Alencar, T. V.; Barboza, A. P.; Mak, K. F.; de Paula, A. M. Observation of Intense Second Harmonic Generation from MoS_2 Atomic Crystals. *Phys. Rev. B: Condens. Matter Mater. Phys.* **2013**, *87*, 201401(R).
14. Li, Y.; Rao, Y.; Mak, K. F.; You, Y.; Wang, S.; Dean, C. R.; Heinz, T. F. Probing Symmetry Properties of Few-Layer MoS_2 and h-BN by Optical Second-Harmonic Generation. *Nano Lett.* **2013**, *13*, 3329–3333.
15. Hendry, E.; Hale, P. J.; Moger, J.; Savchenko, A. K.; Mikhailov, S. A. Coherent Nonlinear Optical Response of Graphene. *Phys. Rev. Lett.* **2010**, *105*, 097401.
16. Wang, G.; Zhang, S.; Zhang, X.; Zhang, L.; Cheng, Y.; Fox, D.; Zhang, H.; Coleman, J. N.; Blau, W. J.; Wang, J. Tunable Nonlinear Refractive Index of Two-Dimensional MoS_2, WS_2, and $MoSe_2$ Nanosheet Dispersions. *Photonics Res.* **2015**, *3*, A51–A55.
17. Zhan, Y.; Liu, Z.; Najmaei, S.; Ajayan, P. M.; Lou, J. Large-Area Vapor-Phase Growth and Characterization of MoS_2 Atomic Layers on a SiO_2 Substrate. *Small* **2012**, *8*, 966–971.
18. Gatensby, R.; McEvoy, N.; Lee, K.; Hallam, T.; Berner, N. C.; Rezvani, E.; Winters, S.; O'Brien, M.; Duesberg, G. S. Controlled Synthesis of Transition Metal Dichalcogenide Thin Films for Electronic Applications. *Appl. Surf. Sci.* **2014**, *297*, 139–146.

19. Berkdemir, A.; Gutiérrez, H. R.; Botello-Méndez, A. R.; Perea-López, N.; Elías, A. L.; Chia, C.-I.; Wang, B.; Crespi, V. H.; López-Urías, F.; Charlier, J.-C.; et al. Identification of Individual and Few Layers of WS_2 Using Raman Spectroscopy. *Sci. Rep.* **2013**, *3*, 1755.
20. Lee, Y.-H.; Zhang, X.-Q.; Zhang, W.; Chang, M.-T.; Lin, C.-T.; Chang, K.-D.; Yu, Y.-C.; Wang, J. T.-W.; Chang, C.-S.; Li, L.-J.; et al. Synthesis of Large-Area MoS_2 Atomic Layers with Chemical Vapor Deposition. *Adv. Mater.* **2012**, *24*, 2320–2325.
21. Zhang, Y.; Zhang, Y.; Ji, Q.; Ju, J.; Yuan, H.; Shi, J.; Gao, T.; Ma, D.; Liu, M.; Chen, Y.; et al. Controlled Growth of High-Quality Monolayer WS_2 Layers on Sapphire and Imaging Its Grain Boundary. *ACS Nano* **2013**, *7*, 8963–8971.
22. Gutiérrez, H. R.; Perea-López, N.; Elías, A. L.; Berkdemir, A.; Wang, B.; Lv, R.; López-Urías, F.; Crespi, V. H.; Terrones, H.; Terrones, M. Extraordinary Room-Temperature Photoluminescence in Triangular WS_2 Monolayers. *Nano Lett.* **2013**, *13*, 3447–3454.
23. Yim, C.; O'Brien, M.; McEvoy, N.; Winters, S.; Mirza, I.; Lunney, J. G.; Duesberg, G. S. Investigation of the Optical Properties of MoS_2 Thin Films Using Spectroscopic Ellipsometry. *Appl. Phys. Lett.* **2014**, *104*, 103114.
24. Li, H.; Zhang, Q.; Yap, C. C. R.; Tay, B. K.; Edwin, T. H. T.; Olivier, A.; Baillargeat, D. From Bulk to Monolayer MoS_2: Evolution of Raman Scattering. *Adv. Funct. Mater.* **2012**, *22*, 1385–1390.
25. Lee, C.; Yan, H.; Brus, L. E.; Heinz, T. F.; Hone, J.; Ryu, S. Anomalous Lattice Vibrations of Single- and Few-Layer MoS_2. *ACS Nano* **2010**, *4*, 2695–2700.
26. Zhao, W.; Ghorannevis, Z.; Amara, K. K.; Pang, J. R.; Toh, M.; Zhang, X.; Kloc, C.; Tan, P. H.; Eda, G. Lattice Dynamics in Mono- and Few-Layer Sheets of WS_2 and WSe_2. *Nanoscale* **2013**, *5*, 9677–9683.
27. Feng, Y.; Dong, N.; Wang, G.; Li, Y.; Zhang, S.; Wang, K.; Zhang, L.; Blau, W. J.; Wang, J. Saturable Absorption Behavior of Free-Standing Graphene Polymer Composite Films Over Broad Wavelength and Time Ranges. *Opt. Express* **2015**, *23*, 559–569.
28. Kumar, S.; Anija, M.; Kamaraju, N.; Vasu, K. S.; Subrahmanyam, K. S.; Sood, A. K.; Rao, C. N. R. Femtosecond Carrier Dynamics and Saturable Absorption in Graphene Suspensions. *Appl. Phys. Lett.* **2009**, *95*, 191911.
29. Braga, D.; Lezama, I. G.; Berger, H.; Morpurgo, A. F. Quantitative Determination of the Band Gap of WS_2 with Ambipolar Ionic Liquid-Gated Transistors. *Nano Lett.* **2012**, *12*, 5218–5223.
30. Yun, W. S.; Han, S. W.; Hong, S. C.; Kim, I. G.; Lee, J. D. Thickness and Strain Effects on Electronic Structures of Transition Metal Dichalcogenides: 2H-MX_2 Semiconductors (M = Mo, W; X = S, Se, Te). *Phys. Rev. B: Condens. Matter Mater. Phys.* **2012**, *85*, 033305.
31. Zhao, W.; Ghorannevis, Z.; Chu, L.; Toh, M.; Kloc, C.; Tan, P.-H.; Eda, G. Evolution of Electronic Structure in Atomically Thin Sheets of WS_2 and WSe_2. *ACS Nano* **2013**, *7*, 791–797.
32. Sheik-Bahae, M.; Said, A. A.; Wei, T.-H.; Hagan, D. J.; Van Stryland, E. W. Sensitive Measurement of Optical Nonlinearities Using a Single Beam. *IEEE J. Quantum Electron.* **1990**, *26*, 760–769.
33. Janisch, C.; Wang, Y.; Ma, D.; Mehta, N.; Elías, A. L.; Perea-López, N.; Terrones, M.; Crespi, V.; Liu, Z. Extraordinary Second Harmonic Generation in Tungsten Disulfide Monolayers. *Sci. Rep.* **2014**, *4*, 5530.
34. Zeng, H.; Liu, G.-B.; Dai, J.; Yan, Y.; Zhu, B.; He, R.; Xie, L.; Xu, S.; Chen, X.; Yao, W.; et al. Optical Signature of Symmetry Variations and Spin-Valley Coupling in Atomically Thin Tungsten Dichalcogenides. *Sci. Rep.* **2013**, *3*, 1608.
35. Wang, G.; Marie, X.; Gerber, I.; Amand, T.; Lagarde, D.; Bouet, L.; Vidal, M.; Balocchi, A.; Urbaszek, B. Giant Enhancement of the Optical Second-Harmonic Emissions of WSe_2 Monolayers by Laser Excitation at Exciton Resonances. *Phys. Rev. Lett.* **2015**, *114*, 097403.
36. He, K.; Kumar, N.; Zhao, L.; Wang, Z.; Mak, K. F.; Zhao, H.; Shan, J. Tightly Bound Excitons in Monolayer WSe_2. *Phys. Rev. Lett.* **2014**, *113*, 026803.
37. Trolle, M. L.; Seifert, G.; Pedersen, T. G. Theory of Excitonic Second-Harmonic Generation in Monolayer MoS_2. *Phys. Rev. B: Condens. Matter Mater. Phys.* **2014**, *89*, 235410.
38. Grüning, M.; Attaccalite, C. Second Harmonic Generation in h-BN and MoS_2 Monolayer: Role of Electron-Hole Interaction. *Phys. Rev. B: Condens. Matter Mater. Phys.* **2014**, *89*, 081102(R).
39. Boggess, T. F.; Bohnert, K. M.; Mansour, K.; Moss, S. C.; Boyd, I. W.; Smirl, A. L. Simultaneous Measurement of the Two-Photon Coefficient and Free-Carrier Cross Section Above the Bandgap of Crystalline Silicon. *IEEE J. Quantum Electron.* **1986**, *22*, 360–368.
40. Van Stryland, E. W.; Vanherzeele, H.; Woodall, M. A.; Soileau, M. J.; Smirl, A. L.; Guha, S.; Boggess, T. F. Two Photon Absorption, Nonlinear Refraction, and Optical Limiting in Semiconductors. *Opt. Eng.* **1985**, *24*, 613–623.
41. Bechtel, J. H.; Smith, W. L. Two-Photon Absorption in Semiconductors with Picosecond Laser Pulses. *Phys. Rev. B* **1976**, *13*, 3515–3522.
42. Yang, H.; Feng, X.; Wang, Q.; Huang, H.; Chen, W.; Wee, A. T. S.; Ji, W. Giant Two-Photon Absorption in Bilayer Graphene. *Nano Lett.* **2011**, *11*, 2622–2627.
43. Ramasubramaniam, A. Large Excitonic Effects in Monolayers of Molybdenum and Tungsten Dichalcogenides. *Phys. Rev. B: Condens. Matter Mater. Phys.* **2012**, *86*, 115409.
44. Qiu, D. Y.; da Jornada, F. H.; Louie, S. G. Optical Spectrum of MoS_2: Many-Body Effects and Diversity of Exciton States. *Phys. Rev. Lett.* **2013**, *111*, 216805.
45. Mak, K. F.; Lee, C.; Hone, J.; Shan, J.; Heinz, T. F. Atomically Thin MoS_2: a New Direct-Gap Semiconductor. *Phys. Rev. Lett.* **2010**, *105*, 136805.
46. Splendiani, A.; Sun, L.; Zhang, Y.; Li, T.; Kim, J.; Chim, C.-Y.; Galli, G.; Wang, F. Emerging Photoluminescence in Monolayer MoS_2. *Nano Lett.* **2010**, *10*, 1271–1275.
47. Lami, J.-F.; Gilliot, P.; Hirlimann, C. Observation of Interband Two-Photon Absorption Saturation in CdS. *Phys. Rev. Lett.* **1996**, *77*, 1632–1635.
48. Gu, B.; Fan, Y.-X.; Chen, J.; Wang, H.-T.; He, J.; Ji, W. Z-Scan Theory of Two-Photon Absorption Saturation and Experimental Evidence. *J. Appl. Phys.* **2007**, *102*, 083101.
49. Li, Y.; Dong, N.; Zhang, S.; Zhang, X.; Feng, Y.; Wang, K.; Zhang, L.; Wang, J. Giant Two-Photon Absorption in Monolayer MoS_2. *Laser & Photon. Rev.* **2015**, DOI: 10.1002/lpor.201500052.
50. Woodward, R. I.; Kelleher, E. J. R.; Howe, R. C. T.; Hu, G.; Torrisi, F.; Hasan, T.; Popov, S. V.; Taylor, J. R. Tunable Q-Switched Fiber Laser Based on Saturable Edge-State Absorption in Few-Layer Molybdenum Disulfide (MoS_2). *Opt. Express* **2014**, *22*, 31113–31122.
51. Li, S.-L.; Miyazaki, H.; Song, H.; Kuramochi, H.; Nakaharai, S.; Tsukagoshi, K. Quantitative Raman Spectrum and Reliable Thickness Identification for Atomic Layers on Insulating Substrate. *ACS Nano* **2012**, *6*, 7381–7388.
52. Liu, H.-L.; Shen, C.-C.; Su, S.-H.; Hsu, C.-L.; Li, M.-Y.; Li, L.-J. Optical Properties of Monolayer Transition Metal Dichalcogenides Probed by Spectroscopic Ellipsometry. *Appl. Phys. Lett.* **2014**, *105*, 201905.
53. Fujiwara, H. *Spectroscopic Ellipsometry: Principles and Applications*; John Wiley & Sons Ltd.: New York, 2007; pp 81−87.
54. Jellison, G. E.; Modine, F. A. Parameterization of the Optical Functions of Amorphous Materials in the Interband Region. *Appl. Phys. Lett.* **1996**, *69*, 371.